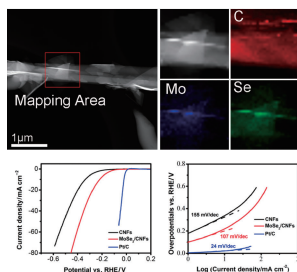


# Synthesis of MoSe<sub>2</sub>/Carbon Nanofibers Hybrid and Its Hydrogen Evolution Reaction Performance

Hui Yang, TingTing Yang, Han Zhu, Ming Zhang, and MingLiang Du\*  
*Faculty of Materials and Textiles, Zhejiang Sci-Tech University, HangZhou 310018, P. R. China*

(E-mail: du@zstu.edu.cn)



MoSe<sub>2</sub>/carbon nanofibers (CNFs) hybrid was synthesized via chemical vapor deposition. Due to the increased surface area and maximally exposed MoSe<sub>2</sub> edges, the hybrid is expected to possess significantly improved catalytic activity. The MoSe<sub>2</sub>/CNFs hybrid was directly used as working electrode for hydrogen evolution reaction and exhibited significantly enhanced catalytic activity.

REPRINTED FROM

**Chemistry  
Letters**

Vol.45 No.1 2016 p.69–71

CMLTAG  
January 5, 2016

The Chemical Society of Japan

## Synthesis of MoSe<sub>2</sub>/Carbon Nanofibers Hybrid and Its Hydrogen Evolution Reaction Performance

Hui Yang, TingTing Yang, Han Zhu, Ming Zhang, and MingLiang Du\*

Faculty of Materials and Textiles, Zhejiang Sci-Tech University, HangZhou 310018, P. R. China

(E-mail: du@zstu.edu.cn)

We present a facile method of growing MoSe<sub>2</sub> on carbon nanofibers (CNFs) via chemical vapor deposition (CVD). Polyacrylonitrile (PAN) was electrospun into nanofibrous mats and graphitized to form CNFs. Subsequent selenization of MoO<sub>3</sub> in a CVD system on the surface of the CNFs produced MoSe<sub>2</sub>/CNFs hybrid. Scanning and transmission electron microscope (SEM and TEM) images revealed large-area MoSe<sub>2</sub> nanosheets attached to the CNFs and indicated that the synthesized MoSe<sub>2</sub>/CNFs hybrids were highly crystalline. Such a structure should increase the surface area and maximally expose the MoSe<sub>2</sub> edges, which may boost catalytic activity. The MoSe<sub>2</sub>/CNFs hybrid was directly used as working electrode for hydrogen evolution reaction (HER) and exhibited significantly enhanced catalytic activity. The onset potential, the over-potential at a current density of 10 mA cm<sup>-2</sup>, and Tafel slope of the MoSe<sub>2</sub>/CNFs hybrid were -69 mV, -219 mV, and 107 mV decade<sup>-1</sup>, respectively. The results suggest that the MoSe<sub>2</sub>/CNFs hybrid can serve as effective and promising catalyst for HER.

Hydrogen, a promising efficient, clean, and sustainable energy carrier, is believed to be the solution to the global energy shortage.<sup>1</sup> Water splitting is the most effective and facile method to produce hydrogen.<sup>2</sup> Traditionally, members of the Pt group have been regarded as the best electrochemical catalysts for hydrogen evolution reactions (HER); however, their cost and scarcity limit their extensive application. Therefore, novel and abundant HER catalysts are highly desired.

Recently, transition metal dichalcogenides (TMDs), having the formula MX<sub>2</sub>, have attracted more attention. They possess weak van der Waals forces between molecular layers and strong chemical bonding within the layers.<sup>3</sup> Due to their special layered structures and properties, TMDs have numerous applications in fields such as catalysis, energy storage, dry lubrication, and photochemical solar cells.<sup>4-6</sup> More recently, studies have suggested that layered TMDs also can serve as efficient electrocatalysts for HER, and numerous studies have focused on TMDs such as MoS<sub>2</sub>, WS<sub>2</sub>, and WSe<sub>2</sub>. However, investigations of hybrids of MoSe<sub>2</sub> and carbon nanofibers (CNFs) have seldom been reported. Cui et al. developed a process to convert molybdenum films to molybdenum dichalcogenide films by e-beam evaporation in a horizontal tube furnace.<sup>7</sup> The edge-terminated MoS<sub>2</sub> and MoSe<sub>2</sub> films exhibited enhanced HER activity. In addition, they investigated the vertical layer orientations of MoSe<sub>2</sub> and WSe<sub>2</sub> on curved and rough surfaces such as nanowires and microfibers.<sup>8</sup> The results indicated that such oriented structures expose the edges of the nanofilms, leading to significantly increased HER activity and extremely high stability. Chen et al. fabricated a unique MoSe<sub>2</sub>/graphene hybrid through in situ growth of GN and MoSe<sub>2</sub> nanosheets on a graphite disc substrate using plasma-enhanced chemical vapor

deposition (PECVD) and the CVD method consecutively. The hybrid exhibited greatly enhanced catalytic activity and outstanding stability.<sup>1</sup>

Recent studies on MoSe<sub>2</sub> synthesis have used the same CVD methods.<sup>6,9,10</sup> These studies used reaction temperature of up to 800–820 °C and a gas mixture of Ar and H<sub>2</sub> in which H<sub>2</sub> functioned as the additional reducing agent.<sup>9</sup>

The edges of the TMDs are well-known active sites for HER; it is therefore essential to expose the edges as much as possible. Various methods have been reported to synthesize TMDs such as liquid exfoliation, lithium-based chemical exfoliation,<sup>11,12</sup> and CVD. To date, CVD is the most effective method to synthesize TMDs. However, the majority of studies have focused on MoS<sub>2</sub>. Se has a lower chemical activity compared with S, making it relatively challenging to synthesize MoSe<sub>2</sub>.

In this study, we present a facile method to fabricate a MoSe<sub>2</sub>/CNFs hybrid. PAN was electrospun into nanofibrous mats and then graphitized to form CNFs. MoSe<sub>2</sub> was then synthesized on CNF surface by the selenization of MoO<sub>3</sub>. The fabricated MoSe<sub>2</sub>/CNF hybrid was directly used as the working electrode for HER and the catalytic performance was evaluated and discussed.

The morphology of the large-area MoSe<sub>2</sub>/CNFs hybrid is shown in Figure 1. As shown in Figure 1a, the CNFs are covered by large amounts of MoSe<sub>2</sub>, and the MoSe<sub>2</sub> nanosheets are stacked together. As shown in Figure 1b, the triangle-layered MoSe<sub>2</sub> stacked together and grew vertically onto CNFs, maximally exposing their edge sites. TEM images of the MoSe<sub>2</sub>/CNFs hybrid are shown in Figure 1c and indicate that the diameter of the CNFs is approximately several hundred nanometers and the length of the triangular MoSe<sub>2</sub> is greater than 500 nm. Furthermore, some defects can be found in the layered MoSe<sub>2</sub>. Lattice fringes can be observed via HRTEM, as shown in the inset of Figure 1c, and the expected alternating brighter (2 Se) and darker (Mo) sites are clearly observed in the images.<sup>10</sup> Figure 1d indicates that MoSe<sub>2</sub> layers are stacked together and that approximately three layers and two crystal planes are intertwined. The SAED image (inset of Figure 1d) indicates that MoSe<sub>2</sub> is monocrystalline. High-angle annular dark-field-scanning transmission electron microscopy and energy-dispersive X-ray spectroscopy were utilized to verify the elemental distribution of the MoSe<sub>2</sub>/CNFs hybrid and the results indicate that the elemental distribution is consistent with the successful formation of layered MoSe<sub>2</sub> covering the CNFs (Figures 1e and 1f).

XPS analysis was used to identify the chemical state of the MoSe<sub>2</sub>/CNFs hybrid. As shown in Figure 2, the 3d spectrum of Mo and Se in the sample indicates that Mo and Se are stoichiometric. Figure 2a shows characteristic Mo3d<sub>5/2</sub> and Mo3d<sub>3/2</sub> peaks located at ca. 229.2 and 232.4 eV, respectively. As reported, the peaks of Mo3d<sub>5/2</sub> and Mo3d<sub>3/2</sub> of MoO<sub>3</sub> were identified at 233.1 and 236.2 eV, respectively,<sup>13</sup> indicating the

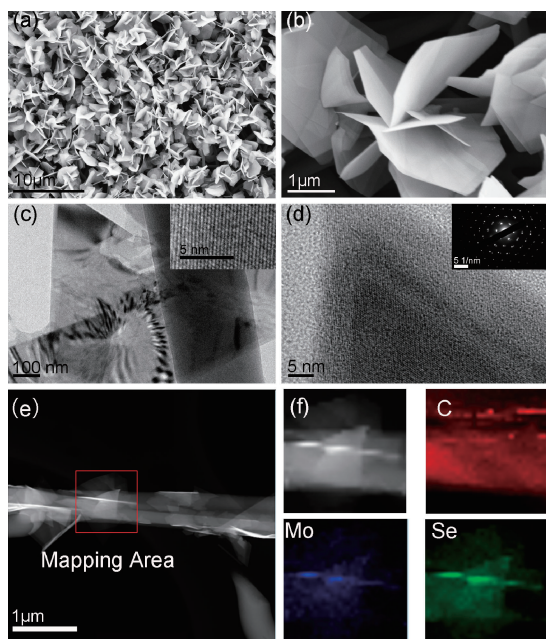


**Figure 1.** The morphology of MoSe<sub>2</sub>/CNFs and high-angle annular dark field scanning transmission electron microscope (HAADF-STEM) images. (a), (b) SEM images of MoSe<sub>2</sub>/CNFs; (c) TEM image of MoSe<sub>2</sub> (inset, HRTEM of MoSe<sub>2</sub>); (d) TEM image of triangle MoSe<sub>2</sub> nanosheets and corresponding select area electron diffraction (SAED, inset of (d)). (e) HAADF-STEM image of MoSe<sub>2</sub>/CNFs and (f) STEM-EDS (energy-dispersive X-ray spectroscopy) mapping images of the selected area.

reduction from Mo<sup>6+</sup> to Mo<sup>4+</sup>.<sup>10</sup> The spectrum of Se was split into Se3d<sub>5/2</sub> and Se3d<sub>3/2</sub> with peaks located at approximately 54.8 and 55.6 eV, respectively, as shown in Figure 2b, confirming the  $-2$  oxidation state of selenium. In addition, the molar ratio of Mo:Se is approximately 1:2. The XRD pattern shown in Figure 2c reveals more details about the crystal structure of the MoSe<sub>2</sub>/CNFs hybrid. The diffraction peak located at 22.2° is ascribed to the CNFs crystalline phase (002) and indicates the presence of crystalline graphitic carbon in the hybrid. Additionally, three peaks can be observed at  $2\theta$  values of approximately 37.3, 43.7, and 63.8° and are attributed to the (103), (105), and (110) planes of MoSe<sub>2</sub>,<sup>14</sup> respectively, confirming the presence of crystalline MoSe<sub>2</sub> in the hybrid material. Figure 2d presents the normal vibrational modes of the MoSe<sub>2</sub>/CNFs hybrid. The two peaks located at 237 and 281 cm<sup>-1</sup> are attributed to A<sub>1g</sub> and E<sub>2g</sub><sup>1</sup>, respectively. The out-of-plane vibrational mode A<sub>1g</sub> is much stronger than in-plane mode E<sub>2g</sub><sup>1</sup> and the intensity ratio of A<sub>1g</sub> to E<sub>2g</sub><sup>1</sup> is approximately 11, indicating the formation of an edge-terminated MoSe<sub>2</sub> structure.<sup>15</sup> In addition, the D and G bands of CNFs located in 1328 and 1590 cm<sup>-1</sup>, respectively, are observed.<sup>16</sup>

Generally, HER consists of two processes. One is the discharge step (Volmer reaction), in which protons are adsorbed to catalysts and form adsorbed hydrogen atoms. It is followed by the desorption process (Heyrovsky reaction) or the combination process (Tafel reaction).<sup>8,14</sup> The HER electrocatalytic activities of the MoSe<sub>2</sub>/CNFs hybrid were evaluated using a typical three-electrode system. The MoSe<sub>2</sub>/CNFs hybrid was used as the

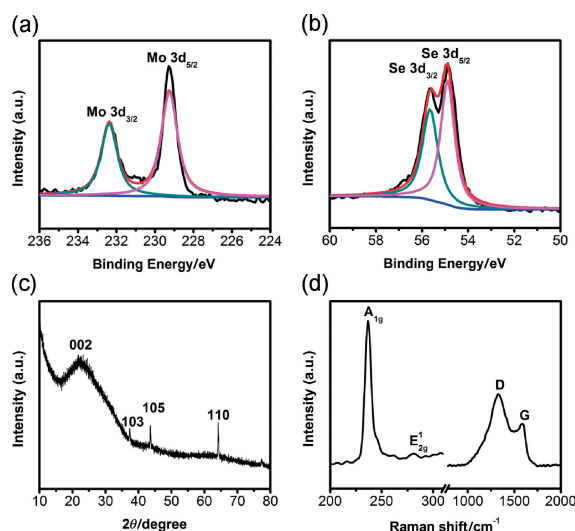


**Figure 2.** (a) XPS spectra of Mo3d and (b) Se3d, (c) XRD pattern, and (d) Raman spectra of MoSe<sub>2</sub>/CNFs hybrid.

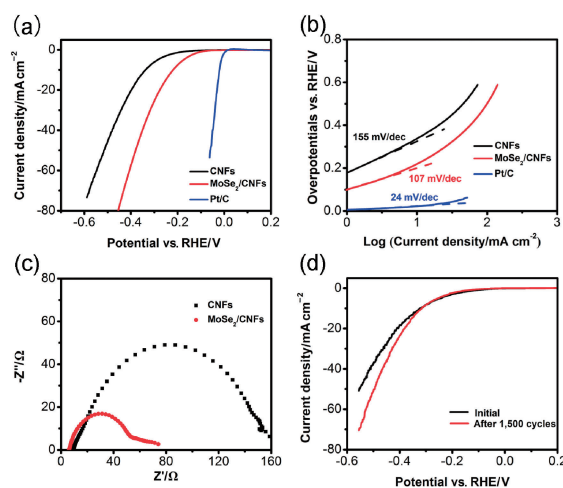


**Figure 3.** HER catalytic activity of MoSe<sub>2</sub>/CNFs hybrid. (a) Polarization curves of pure CNFs and MoSe<sub>2</sub>/CNFs hybrid. (b) Corresponding Tafel plot. (c) Nyquist plots of electrochemical impedance spectra (EIS) for pure CNFs and MoSe<sub>2</sub>/CNFs hybrid and (d) electrochemical stability test of MoSe<sub>2</sub>/CNFs hybrid.

working electrode and a platinum net electrode and a saturated calomel electrode served as the counter electrode and the reference electrode, respectively. All experiments were performed in 0.5 M H<sub>2</sub>SO<sub>4</sub> solution. The HER activity was evaluated by linear-sweep voltammetry and all the polarization curves were obtained after iR-compensation.

In this study, the onset potential of the MoSe<sub>2</sub>/CNFs hybrid is presented in comparison with pure CNFs. The polarization curves of pure CNFs and the MoSe<sub>2</sub>/CNFs hybrid are shown in Figure 3a. The MoSe<sub>2</sub>/CNFs hybrid exhibits a much lower onset potential than that of pure CNFs:  $-69$  and  $-161$  mV vs. reversible hydrogen electrode (RHE), respectively. In the case of the MoSe<sub>2</sub>/CNFs hybrid, the over-potential reaches approximately  $-219$  mV (vs. RHE) at a current density of 10 mA cm<sup>-2</sup> ( $J = 10$  mA cm<sup>-2</sup>). In comparison, the over-potential of pure

CNFs is  $-336$  mV vs. RHE ( $J = 10$  mA cm $^{-2}$ ), which is much higher than the MoSe $_2$ /CNFs hybrid. The Tafel slope of pure CNFs and MoSe $_2$ /CNFs hybrid are shown in Figure 3b. The linear part of the MoSe $_2$ /CNFs hybrid slope is fitted to attain a slope of  $107$  mV decade $^{-1}$  and the Tafel slope of pure CNFs is approximately  $155$  mV decade $^{-1}$ , which indicates that the rate-determining step of the MoSe $_2$ /CNFs hybrid in HER is the Volmer reaction.<sup>7,17,18</sup>

Furthermore, to evaluate the charge-transfer resistance ( $R_{ct}$ ) of pure CNFs and the MoSe $_2$ /CNFs hybrid, electrochemical impedance spectra (EIS) for both materials were obtained. The Nyquist plots of the EIS for the two materials are shown in Figure 3c. They indicate that the MoSe $_2$ /CNFs hybrid exhibits a much smaller arc than pure CNFs, demonstrating higher reaction rate in HER.

In addition, stability is another critical factor related to the activity of HER. In this study, we assessed the stability of the MoSe $_2$ /CNFs hybrid by acquiring continuous cyclic voltammograms (CV) for 1500 cycles at the scanning rate of  $100$  mV s $^{-1}$ . The polarization curves before and after cycling are evaluated by linear-sweep voltammetry with a lower scanning rate of  $2$  mV s $^{-1}$ . As shown in Figure 3d, the current density after cycling is much higher than before cycling, probably due to further activation of the catalyst during the water splitting process.

In summary, a MoSe $_2$ /CNFs hybrid was synthesized successfully via a facile CVD step. CNFs was employed as both a substrate and an electron mediator. The results demonstrated that large-area MoSe $_2$  was deposited on the CNFs and highly crystalline MoSe $_2$ /CNFs hybrids were synthesized. Such a structure is expected to increase the surface area and maximally expose the edges of MoSe $_2$ , which may boost the catalytic activity. The MoSe $_2$ /CNFs hybrid was directly used as working electrode for HER and exhibited significantly enhanced catalytic activity. The onset potential, the over-potential at a current density of  $10$  mA cm $^{-2}$ , and Tafel slope of the MoSe $_2$ /CNFs hybrid were  $-69$  mV,  $-219$  mV, and  $107$  mV decade $^{-1}$ , respectively. The results suggest that the MoSe $_2$ /CNFs hybrid can serve as an effective and promising catalyst for HER.

This study was supported by the National Natural Science Foundation of China (NSFC) (Grant Nos. 51373154 and 51573166), Program for Innovative Research Team of Zhejiang Sci-Tech University and the 521 Talent Project of Zhejiang Sci-Tech University.

Supporting Information is available on <http://dx.doi.org/10.1246/cl.150844>.

## References

- 1 S. Mao, Z. Wen, S. Ci, X. Guo, K. Ostrikov, J. Chen, *Small* **2015**, *11*, 414.
- 2 J. Greeley, T. F. Jaramillo, J. Bonde, I. Chorkendorff, J. K. Nørskov, *Nat. Mater.* **2006**, *5*, 909.
- 3 V. Kiran, D. Mukherjee, R. N. Jenjeti, S. Sampath, *Nanoscale* **2014**, *6*, 12856.
- 4 C. Fan, Z. Wei, S. Yang, J. Li, *RSC Adv.* **2014**, *4*, 775.
- 5 J. Xia, X. Huang, L.-Z. Liu, M. Wang, L. Wang, B. Huang, D.-D. Zhu, J.-J. Li, C.-Z. Gu, X.-M. Meng, *Nanoscale* **2014**, *6*, 8949.
- 6 X. Lu, M. I. B. Utama, J. Lin, X. Gong, J. Zhang, Y. Zhao, S. T. Pantelides, J. Wang, Z. Dong, Z. Liu, W. Zhou, Q. Xiong, *Nano Lett.* **2014**, *14*, 2419.
- 7 D. Kong, H. Wang, J. J. Cha, M. Pasta, K. J. Koski, J. Yao, Y. Cui, *Nano Lett.* **2013**, *13*, 1341.
- 8 H. Wang, D. Kong, P. Johannes, J. J. Cha, G. Zheng, K. Yan, N. Liu, Y. Cui, *Nano Lett.* **2013**, *13*, 3426.
- 9 J. C. Shaw, H. Zhou, Y. Chen, N. O. Weiss, Y. Liu, Y. Huang, X. Duan, *Nano Res.* **2014**, *7*, 511.
- 10 X. Wang, Y. Gong, G. Shi, W. L. Chow, K. Keyshar, G. Ye, R. Vajtai, J. Lou, Z. Liu, E. Ringe, B. K. Tay, P. M. Ajayan, *ACS Nano* **2014**, *8*, 5125.
- 11 J. N. Coleman, M. Lotya, A. O'Neill, S. D. Bergin, P. J. King, U. Khan, K. Young, A. Gaucher, S. De, R. J. Smith, I. V. Shvets, S. K. Arora, G. Stanton, H.-Y. Kim, K. Lee, G. T. Kim, G. S. Duesberg, T. Hallam, J. J. Boland, J. J. Wang, J. F. Donegan, J. C. Grunlan, G. Moriarty, A. Shmeliov, R. J. Nicholls, J. M. Perkins, E. M. Grieveson, K. Theuvsissen, D. W. McComb, P. D. Nellist, V. Nicolosi, *Science* **2011**, *331*, 568.
- 12 Z. Zeng, T. Sun, J. Zhu, X. Huang, Z. Yin, G. Lu, Z. Fan, Q. Yan, H. H. Hng, H. Zhang, *Angew. Chem., Int. Ed.* **2012**, *51*, 9052.
- 13 G. W. Shim, K. Yoo, S.-B. Seo, J. Shin, D. Y. Jung, I.-S. Kang, C. W. Ahn, B. J. Cho, S.-Y. Choi, *ACS Nano* **2014**, *8*, 6655.
- 14 H. Tang, K. Dou, C.-C. Kaun, Q. Kuang, S. Yang, *J. Mater. Chem. A* **2014**, *2*, 360.
- 15 X. Zheng, J. Xu, K. Yan, H. Wang, Z. Wang, S. Yang, *Chem. Mater.* **2014**, *26*, 2344.
- 16 H. Zhu, F. Lyu, M. Du, M. Zhang, Q. Wang, J. Yao, B. Guo, *ACS Appl. Mater. Interfaces* **2014**, *6*, 22126.
- 17 N. Pentland, J. O'M. Bockris, E. Sheldon, *J. Electrochem. Soc.* **1957**, *104*, 182.
- 18 B. E. Conway, B. V. Tilak, *Electrochim. Acta* **2002**, *47*, 3571.